SUPPORTING INFORMATION

Electronic Supplementary Information (ESI)

Reductive Surfactant-Assisted One-Step Fabrication of $BiOI/BiOIO_3$ Heterojunction Biophotocatalyst for Enhanced Photodynamic Theranostics Overcoming Tumor Hypoxia

Wenyao Zhen,[a,b] Yang Liu,[b,c] Xiaodan Jia,[a] Lie Wu,[a] Chao Wang[a,b] and Xiue Jiang*[,a,b]

[a]State Key Laboratory of Electroanalytical Chemistry, Changchun Institute of Applied Chemistry, Chinese Academy of Sciences, Changchun 130022, Jilin, People's Republic of China.
[b]University of Science and Technology of China, Hefei 230026, Anhui, People's Republic of China.
[c]State Key Laboratory of Rare Earth Resource Utilization, Changchun Institute of Applied Chemistry, Chinese Academy of Sciences, Changchun 130022, Jilin, People's Republic of China

Experimental Procedures

Chemicals and Reagents: Pentaerythritol tetrakis 3-mercaptopropionate (PTMP), $Bi(NO_3)_3 \bullet 5H_2O$, KIO_3, KI, methacrylic acid (MAA), 5,5',6,6'-tetrachloro-1,1',3,3'-tetraethyl-benzimidazolylcarbocy anine iodide (JC-1), methyl thiazolyl tetrazolium (MTT), calcein acetoxymethyl ester (Calcein AM), propidium iodide (PI), 1,3-diphenylisobenzofuran (DPBF), 4,6-diamidino-2-phenylindole (DAPI), fluorescein isothiocyanate (FITC), methyl red (MR), 2,7-dichlorofluorescin diacetate (DCFH-DA) and $[Ru(dpp)_3]Cl_2$ (RDPP) were obtained from Sigma-Aldrich (America). 2,2'-Azobis(2-methylpropionitrile) (AIBN) was purchased from Shanghai Aladdin Reagent Co. (Shanghai, China). Singlet oxygen sensor green (SOSG) was purchased from Thermo Fisher Scientific Co. (Shanghai, China). Hydroxyphenyl fluorescein (HPF) was purchased from Shanghai Maokang Bio. Co. (Shanghai, China). Dulbecco's modified eagle's medium (DMEM) was purchased from Thermo Scientific Co. (Beijing, China). Standard fetal bovine serum (FBS) was purchased from Tianjin Kangyuan Biology Technology Manufacture Co., Ltd. (Tianjin, China). Hematoxylin-eosin (H&E), mito-tracker green, lyso-tracker red and adenosine 5'-triphosphate (ATP) assay kit were purchased from Beyotime Biotechnology Co., Ltd. (Shanghai, China). Inhibition and produce superoxide anion assay kit and the reduced glutathione assay kit were purchased from Nanjing Jiancheng Bioengineering Institute.

Instruments: TEM images and X-ray energy dispersive spectroscopy (EDS) spectrum were obtained by a FEI TECNAI G2 high-resolution transmission electron microscope operating with a field-emission gun operating at 200 kV. Scanning electron microscope (SEM) image was taken with a XL30 ESEM-FEG field-emission scanning electron microscope (FEL COMPANY, Netherlands). The UV-vis diffuse-reflectance spectrometry (DRS) spectra were obtained for the dry-pressed disk samples using a Hitachi U-3900 spectrometer equipped with an integrating sphere assembly. Nicolet 520 Fourier transform infrared (FTIR) spectrometer was used to obtain FTIR spectra. X-ray photoelectron spectra (XPS) were obtained by ESCALab220i-XL electron spectrometer. X-ray diffraction (XRD) spectrum was gained by a D8 ADVANCE X-ray diffractometer. The exact concentrations of Bi was detected by inductively coupled plasma atomic emission spectroscopy (ICP-AES, Thermo Scientific Xseries 2, Thermo Fisher Scientific, USA).

Preparation of Trithiol-terminated Poly-(methacrylic acid) (PTMP-PMAA): Ethanol (100 mL), MAA monomer (20 g), PTMP (2.267 g) and AIBN (0.19 g) were placed into a round-bottomed flask fitted with a reflux condenser under nitrogen with mechanical stirring, the mixture was reacted at 75^{o}C for 5 h. The solvent was removed by a rotary evaporator (Germany, IKA-RV10 V-C) and the product was isolated by precipitating into ether (4 ^{o}C). The redundant solvent and monomer were removed by evaporation using a vacuum oven at 45 ^{o}C for 72 h.

Preparation of $BiOI/BiOIO_3$ Nanocomposites (BB NCs), $BiOIO_3$ and BiOI: HNO_3 was used to adjust the pH (pH 2.6) of PTMP-PMAA aqueous solution (5.70 mg mL^{-1}). 3 mL of $Bi(NO_3)_3 \cdot 5H_2O$ aqueous solution (0.06 g mL^{-1}) was dropwise added into the above mixture. Then, 3 mL of KIO_3 dispersion aqueous liquid (0.11 g mL^{-1}) was added and stirred for 30 min, the mixture was allowed to react at 180°C for 12 h in an oven. Finally, the products were obtained and further washed by ethanol for three times through centrifuging at 10000 rpm for 10 min and dried at 60°C for further use. The single $BiOIO_3$ was prepared according to above method without the addition of PTMP-PMAA. The single BiOI was also prepared according to above method without the addition of PTMP-PMAA and the KIO_3 was replaced by KI (3 mL, 0.085 g mL^{-1}).

Electrochemical Impedance Spectroscopy Measurements: Metrohm autolab instrument was used to detect the electrochemical impedance. The platinum wire was used as the counter electrode, Ag/AgCl electrode was used as the reference electrode, and 100 μL of BiOI, $BiOIO_3$ or BB NCs suspension (1 mg mL^{-1}) was drop-cast on the cleaned glassy carbon electrodes (GCE) to be served as the working electrode. Prior to that, the GCE was polished with 1.0 and 0.3 μm alumina powder, respectively, followed by sonication in ethanol solution and doubly distilled water successively. Electrochemical impedance spectroscopy experiments were carried out in a home-made three-electrode electrochemical cell. Nyquist plots were detected in 5 mM $K_3[Fe(CN)_6/K_4[Fe(CN)_6]$ (1:1) with 0.1 M KCl solution.

Detection of Mott-Schottky: Mott-Schottky plot was detected in 1 mol L^{-1} Na_2SO_4 aqueous solution with frequencies of 3000 Hz. The Platinum wire was acted as the counter electrode, Ag/AgCl electrode was used as the reference electrode, and 100 μL of BiOI and $BiOIO_3$ suspension (1 mg mL^{-1}) was drop-cast on the cleaned glassy carbon electrodes (GCE) to be acted as working electrode. Then, the impedance at 3000 Hz was detected.

In Vitro Detection of •OH: HPF was used to detect the generation of •OH. Typically, 1 mL BB NCs aqueous solution (80 μg mL^{-1}) containing with HPF (1 μM) were irradiated by 650 nm laser (0.5 W cm^{-2}), the fluorescence of HPF was detected after 15 min. HPF aqueous solution with laser served as control. To demonstrate the addition of H_2O_2 can enhance the generation of •OH, BB NCs dispersion (80 μg mL^{-1}) containing with H_2O_2 (100 μM) and HPF (1 μM) was also irradiated by 650 nm laser (0.5 W cm^{-2}), the fluorescence was detected after 15 min. The fluorescence of HPF in 520 nm (excitation: 488 nm) was measured. Notably, to detect the content of •OH in hypoxia condition, all of the above-mentioned solutions were irradiated by 650 nm laser after aerating the solution with nitrogen for 10 min.

In Vitro Generation of O_2: The content of O_2 was measured by the portable dissolved oxygen meter. Typically, 25 mL of BB NCs aqueous solutions (40, 80 μg mL^{-1}) were irradiated by 650 nm laser (0.5 W cm^{-2}), during the irradiation process, the concentration of the generated O_2 was recorded every 10 seconds.

***In Vitro* Detection of Singlet Oxygen ($^1O_2$) by SOSG:** SOSG was used for detecting the generation of $^1O_2$. Typically, 10 μL of

SOSG solution (50 μM) was added into 1 mL of BB NCs aqueous solution (80 μg mL^{-1}). Then, the mixture was irradiated by 650 nm laser (0.5 W cm^{-2}), the fluorescence in 525 nm (excitation: 488 nm) was measured 15 min. Notably, to detect the content of $^1O_2$ in hypoxia condition, all of the above-mentioned solutions were irradiated by 650 nm laser after aerating the solution with N_2 for ~10 min.

***In Vitro* Detection of Superoxide Anion ($\bullet O_2^-$):** $\bullet O_2^-$ was detected through inhibition and produce superoxide anion assay kit. The BB NCs aqueous solution (80 μg mL^{-1}, 50 mL) was added to 1.3 mL of test solutions, respectively. Then, the mixture was irradiated by 650 nm laser (0.5 W cm^{-2}) for 15 min, and the mixtures were incubated at 37^{o}C for 40 min. Then, the mixture was centrifuged at 10000 rpm. Then, 2 mL of the chromogenic agent was added to above solutions and kept at 25 ^{o}C for 10 min, the absorbance at 550 nm was measured by UV–vis absorption spectroscopy. The BB NCs aqueous solution without the illumination served as control.

***In Vitro* Detection of $\bullet O_2^-$ or $^1O_2$ by DPBF:** DPBF can response to $\bullet O_2^-$ and $^1O_2$, DPBF was employed to evaluate the ROS production of BB NCs by UV-vis absorption spectra. 15 μL of DPBF solution (10 mM in ethanol) was added into 990 μL of BB NCs (80 μg mL^{-1}) ethanol aqueous solution (ethanol: H_2O = 4:6) with or without NaN_3 (10 mM). Then, the mixture was irradiated with a 650 nm laser for 15 min (0.5 W cm^{-2}). Then, the sample was centrifuged at 10000 rpm for 10 min. Afterwards, the absorbance of DPBF at 410 nm was recorded. The group without laser was used as control. Furthermore, BB NCs (80 μg mL^{-1}) ethanol aqueous solution (ethanol: H_2O = 4:6) with p-benzoquinone (BQ, 1 mM) was also detected according to the above procedures.

Detection of •OH by Terephthalic Acid (TA): The detection of •OH was further verified according to the reaction of TA and •OH. 3 mL of BB NCs aqueous solution (80 μg mL^{-1}, 0.1 M acetate buffer (pH = 4.0)*)* containing TA (0.5 mM) was stirred in the darkness for 30 min to establish an adsorption-desorption equilibrium. Then, the mixture was exposed to a 650 nm laser (0.5 W cm^{-2}) for 30 min. After that, above liquid was centrifuged to remove nanomaterials. The changes in the 435 nm fluorescence emission peak were recorded with the excitation wavelength was 315 nm.

Degradation of MR: The generation of •OH was also demonstrated by photodegradation of MR under visible light irradiation (650 nm laser, 0.5 W cm^{-2}). Typically, 10 mg MR was dissolved into 5 mL of DMF. Then, 2.977 mL of BB NCs (80 μg mL^{-1}) aqueous solution was added into 23 μL of MR solution (2 mg mL^{-1}) and the suspensions were stirred in the darkness for 30 min to establish an adsorption-desorption equilibrium. Then, the mixture was exposed to a 650 nm laser (0.5 W cm^{-2}) for different times (0, 5, 10, 20 and 30 min). After that, the above liquid was centrifuged to remove nanomaterials. The absorbance at 522 nm was measured by UV-vis spectroscopy to evaluate the content of MR.

The Evaluation of Photothermal Response of BB NCs: 1 mL of BB NCs aqueous solutions (80 μg mL^{-1}) was added into a

quartz cell and exposed to 650 nm laser (0.5 W cm^{-2}) for 15 min. A thermocouple probe was used to record real-time temperature every 30 s, the temperature variation of H_2O was also detected. Thermal imaging was also recorded through the infrared thermal imaging camera (FLIR E50, Fluke, USA) every 2 min during the irradiation.

Biocompatibility of BB NCs: HeLa cells were seeded into 96-well plates in normoxia (21% O_2) or hypoxia (2% O_2) condition at 37°C for 12 h. BB NCs solutions (0, 25, 50, 100, 200, 300 μg mL^{-1} in DMEM medium) were added into each well and cells were continued to be cultured for another 24 h. Cells were rinsed three times and then 100 μL of MTT PBS solution (0.5 mg mL^{-1}) was added to each well. After that, cells were incubated for another 5 h at 37°C, and PBS was abandoned. Then, 200 μL of DMSO was added into each well and the absorbance at 570 nm was detected by a plate reader.

Cell Uptaken of BB NCs: Firstly, we prepared FITC labeled BB NCs. Typically, 0.5 mL of FITC aqueous solution (2 mg mL^{-1}) was slowly added into 20 mL of BB NCs aqueous solution (200 μg mL^{-1}) and vigorously stirred for 12 h in the dark. Then, the above solution were further washed by water through centrifugation for three times and collected. HeLa cells were seeded into culture dishes and incubated in culture medium in 5% CO_2 at 37°C for 24 h. Then, cells were incubated with 1 mL of FITC-BB NCs (80 μg mL^{-1} in DMEM medium) for 12 h. Then, cells were washed three times with PBS. Cells were further incubated with DAPI (10 μg mL^{-1}, blue) and lyso-tracker red (0.1 μM, red) in DMEM medium for 50 min, then cells were rinsed again with PBS for three times. Afterwards, the fluorescence of cells was imaged using a CLSM. Light emission of DAPI (420 nm ~ 500 nm), lyso-tracker red (580 nm ~ 620 nm), FITC (500 nm ~ 550 nm), at the excitation of 405 nm, 488 nm, 543 nm, 488 nm, and 633 nm, respectively.

The Generation of •OH in HeLa Cells: HeLa cells (2.5×10^4 cells per dish) were seeded into culture dishes and incubated at 37°C in 5% CO_2 for 24 h, respectively. Then, cells were incubated with HPF (10 μM in DMEM medium) for another 40 min. After that, each culture dish was rinsed with PBS for three times and further incubated with 1 mL of BB NCs solution (80 μg mL^{-1} in DMEM medium) for 24 h. The cells were further rinsed three times by PBS, and each culture dish was then added into 1 mL of DMEM medium containing H_2O_2 (100 μM) and irradiated with the 650 nm laser (0.5 W cm^{-2}) for 15 min. Cells were continued to be cultured for another 12 h. After that, the cells were further rinsed three times by PBS and the fluorescence of the cells was imaged with CLSM using an excitation of 488 nm, the emission was collected between 500 and 600 nm. Whatsmore, to distinguish the effects in normoxia and hypoxia condition, we incubated cells in 21% O_2 and 2% O_2 condition, respectively. Cells only with treatment of laser served as control group, and individual H_2O_2/laser-treated and BB NCs/laser-treated cells were also conducted according to above procedures.

The Generation of O_2 in HeLa Cells: HeLa cells were seeded into culture dishes and incubated at 37°C in 5% CO_2 for 24 h, respectively. Then, cells were incubated with RDPP (10 μM in DMEM medium) for 4 h. After that, culture dishes were

washed by PBS and incubated with 1 mL of BB NCs (80 μg mL^{-1} in DMEM medium) for 24 h. The cells were further rinsed three times with PBS, then each culture dish was then added into 1 mL of DMEM medium and irradiated with the 650 nm laser (0.5 W cm^{-2}) for 15 min. Cells were further incubated for 12 h. After that, the cells were washed for three times by PBS and the fluorescence of the cells was imaged with CLSM using an excitation of 488 nm, the emission was collected between 600 and 700 nm. Whatsmore, to distinguish the effects in normoxia and hypoxia condition, we incubated cells in 21% O_2 and 2% O_2 condition, respectively. Cells without treatment of BB NCs or laser served as control group, and individual BB NCs-treated and laser-treated cells were also conducted according to above procedures.

The Generation of $^1O_2$ in HeLa Cells: HeLa cells were seeded into culture dishes and incubated at 37°C in 5% CO_2 for 24 h, respectively. Then, cells were incubated with SOSG (10 μM in DMEM medium) for another 30 min. After that, each culture dish was rinsed with PBS for three times and further incubated with 1 mL of BB NCs solution (80 μg mL^{-1} in DMEM medium) for 24 h. The cells were further rinsed three times with PBS, then each culture dish was then added into 1 mL of DMEM medium and then irradiated with the 650 nm laser (0.5 W cm^{-2}) for 15 min. Cells were continued to be cultured for another 12 h. Finally, the cells were further rinsed three times by PBS and the fluorescence of the cells was imaged with CLSM using an excitation of 488 nm, the emission was collected between 500 and 650 nm. Whatsmore, to distinguish the effects in normoxia and hypoxia condition, we incubated cells in 21% O_2 and 2% O_2 condition, respectively. Cells without treatment of BB NCs or laser served as control group, and individual BB NCs-treated and laser-treated cells were also conducted according to above procedures.

Generation of ROS Detected by DCFH-DA: HeLa cells (2.5 × 10^4 cells per dish) were seeded into culture dishes and incubated at 37°C in 5% CO_2 for 24 h, respectively. Then, cells were incubated with DCFH-DA (10 μM in DMEM medium) for another 30 min. After that, each culture dish was rinsed with PBS for three times and further incubated with 1 mL of BB NCs solution (80 μg mL^{-1} in DMEM medium) for 24 h. The cells were further rinsed for three times with PBS, then each culture dish was then added into 1 mL of DMEM medium and then irradiated with the 650 nm laser (0.5 W cm^{-2}) for 15 min. Cells were continued to be cultured for another 12 h. Finally, the cells were further rinsed three times by PBS and the fluorescence of the cells was imaged with CLSM using an excitation of 488 nm, the emission was collected between 500 and 650 nm. Whatsmore, to distinguish the effects in normoxia and hypoxia condition, we incubated cells in 21% O_2 and 2% O_2 condition, respectively. Cells without treatment of BB NCs or laser served as control group, and individual BB NCs-treated and laser-treated cells were also conducted according to above procedures.

Detection of Mitochondrial Membrane Potential (MMP): The MMP in cells was observed by JC-1 through CLSM. For CLSM imaging, the HeLa cells were seeded in culture dishes at 37°C for 24 h. Then, cells were added into BB NCs (80 μg mL^{-1} in

DMEM medium). After 24 h, the medium was removed and the cells were washed by PBS. After that, 1 mL of DMEM medium were added, cells were irradiated through 650 nm laser (0.5 W cm^{-2}) for 15 min. Subsequently, the cells were incubated for another 12 h and stained by JC-1 (2.5 μg mL^{-1} in PBS) for 20 min at 37°C . After that, the cells were rinsed by JC-1 buffer solution, and investigated by CLSM. The JC-1 monomer was measured on the green emission channel (510 ~ 540 nm), and JC-1 aggregate was measured on the red emission channel (570 ~ 620 nm) at the laser excitation wavelength is 488 nm. Cells without treatment of BB NCs or laser were acted as control, and individual BB NCs-treated and laser-treated cells were also conducted on the basis of above procedures.

***In Vitro* PDT:** HeLa cells were seeded in 96-well plates and incubated according to the above mentioned procedures. Then, cells were incubated with 200 μL of BB NCs with different concentrations (0, 10, 20, 40, 80 μg mL^{-1} in DMEM medium) for 24 h in the same condition, respectively. Then, cells were washed by PBS for three times and 200 μL of fresh DMEM medium was added. Afterwards, cells were exposed to 650 nm laser (0.5 W cm^{-2}) for 15 min. After illumination, cells were incubated for another 12 h. Control group was placed in the same conditions without irradiation. The cell viability was detected by MTT assay and observed on a CLSM stained by Calcein AM (8×10^{-8} M in PBS) and PI (5×10^{-7} M in PBS) for 20 min. Whatsmore, to distinguish the therapeutic effects in normoxia and hypoxia condition, we incubated cells in 21% O_2 and 2% O_2 condition, respectively.

Detection of Adenosine 5'-Triphosphate (ATP) Content: The concentration of intracellular ATP was detected using commercially available ATP assay kit. HeLa cells were seeded into 6-well plates and incubated at 37°C in 5% CO_2 for 24 h. 1 mL of BB NCs (80 μg mL^{-1} in DMEM medium) was added and incubated for 24 h in the same condition. After that, cells were swilled by PBS for three times and 1mL of fresh DMEM medium was added. Afterwards, cells were exposed to 650 nm laser (0.5 W cm^{-2}) for 15 min. After illumination, cells were incubated for another 12 h. After that, cells in each wells were added into 200 μL of cell lysis buffer for 5 min, cells were collected and centrifuged at 12000 rpm for 5 min. ATP content of above supernatant was detected by measuring the luminescence by microplate reader.

Animal Tumor Model and *In Vivo* PDT: Female Kunming mice (20~25 g) were used to obtain the xenograft uterine cervical cancer cells (U14) tumor models. U14 cells in 100 μL of PBS were subcutaneously injected into the right alar area of the mice. While the tumors grow to ~100 mm^3, the mice were divided into four groups: (a) PBS; (b) BB NCs (80 μg mL^{-1}, 200 μL); (c) PBS/Laser and (d) BB NCs (80 μg mL^{-1}, 200 μL). Each mouse was intravenously injected every two days. At 24 h post-injection, tumors of relevant groups were irradiated by 650 nm laser (0.5 W cm^{-2}) for 15 min. On the one hand, the tumor size was detected by digital calliper, tumor volumes were calculated on the basis of the following fomula: $Volume = (Length \times Width^2) \div 2$; on the other hand, the body weight of mice was also recorded every two days to assess

long-term *in vivo* toxicity. At 15th day, some of the tumors at different treatments groups were dissected and weighed.

Histology Staining: While the mice were treated on the 7th day, the tumor tissues were dissected from some of the mice in different treatments and fixed in 10% neutral buffered formalin and processed into paraffin. After some of the mice were treated on the 30th day, the main normal organs were also dissected and treated according to the same procedures . All of the tissues were sliced and stained for hematoxylin and eosin (H&E) staining, all of the tissues were investigated by a digital microscope (Leica QWin). Tumors were also stained by hypoxia-inducible factor (HIF-1α) and investigated.

Detection of Blood Parameters: 12 tumor-bearing mice were used to examine the blood parameters and they were separated into four groups. The mice were conducted as follows: (a) PBS; (b) BB NCs (0.64 mg kg^{-1}); (c) PBS/laser and (d) BB NCs/laser (0.64 mg kg^{-1}), each mouse was intravenously injected. At 24 h post-injection, tumors on mice of treatment group were irradiated by 650 nm laser (0.5 W cm^{-2}) for 15 min. On the 30th day, blood of above mice was collected from the eye socket. The blood of healthy mice was used as control. Then, the complete blood was measured by the automatic blood analyzer using protocols approved by China-Japan union hospital of Jilin University.

CT Imaging: CT imaging was obtained by Philips 256-slice CT scanner (Philips Medical System). BB NCs aqueous solutions with different concentrations (0.32, 0.63, 1.25, 2.5, 5, 10 mg mL^{-1}) were placed in 1.5 mL tubes. For *in vivo* CT imaging, the tumor-bearing mouse was intratumor injected with BB NCs (0.64 mg kg^{-1}). CT images were acquired before and after injection. Images were reformed to coronal images by a computational technique referred to as multiplanar-reconstruction.

Distribution of BB NCs: BB NCs (0.64 mg kg^{-1}) were intravenously injected into the tumor-bearing mice (n = 3). After 24 h, mice were dissected, main normal organs and tumor were collected, organs were weighted and dissolved in digesting aqua regia (HNO_3:HCl = 1:3) for 48 h. The average tumor weight was about 0.1069 g (~100 mm^3). The amounts of Bi in different samples were measured by ICP-AES.

Excretion Trace of BB NCs: BB NCs (0.64 mg kg^{-1}) were intravenously injected into mice (n = 3). And mice were placed in a metabolism cage. The feces and urine were collected and weighted every 12 h, and the contents of Bi were detected by ICP-AES.

Blood Circulation of BB NCs: BB NCs (2.5 mg kg^{-1}, equal to the 1.17 mg kg^{-1} of Bi content) were intravenously injected into the SD rats (300 g), and the blood were collected and weighted at different time points (10 min, 30min, 1h, 2h, 4h, 6h, 8h, 12h, 24 h). The blood samples were weighted and dissolved in digesting aqua regia (HNO_3:HCl = 1:3) for 48 h. The concentrations of Bi in the blood samples were detected by ICP-AES.

Results and Discussion

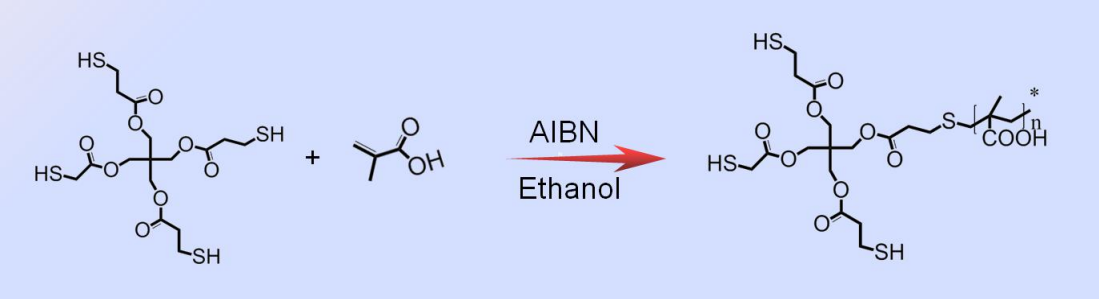

Fig. S1 Schematic illustration of the preparation process of PTMP-PMAA.

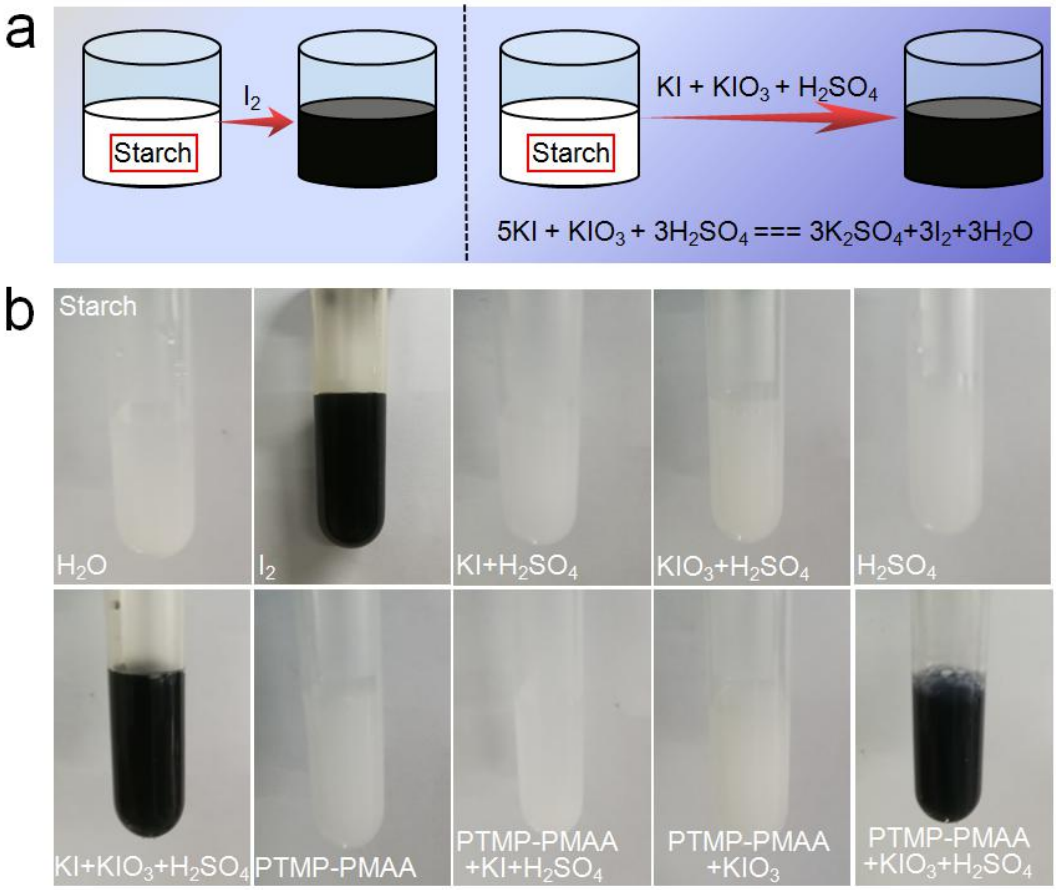

Fig. S2 Demonstration of the generation of I^- during the interaction of PTMP-PMAA with KIO_3.

When starch is mixed with iodine, the starch is highly sensitive color change from brown to blue and have been used to indicate the endpoint of iodine titration.[1] On the other hand, KIO_3 and KI can be converted into iodine by addition of sulfuric acid.[2] The coexistence of I^- and IO_3^- can be identified by using starch as an external indicator, and the reaction is expressed as Figure S2a. In addition, the –SH of our used surfactant (PTMP-PMAA) can reacted with KIO_3 and generate KI (Figure S2b),[3] which can be demonstrated by the blue color showed in the PTMP-PMAA + KIO_3 + H_2SO_4 group.

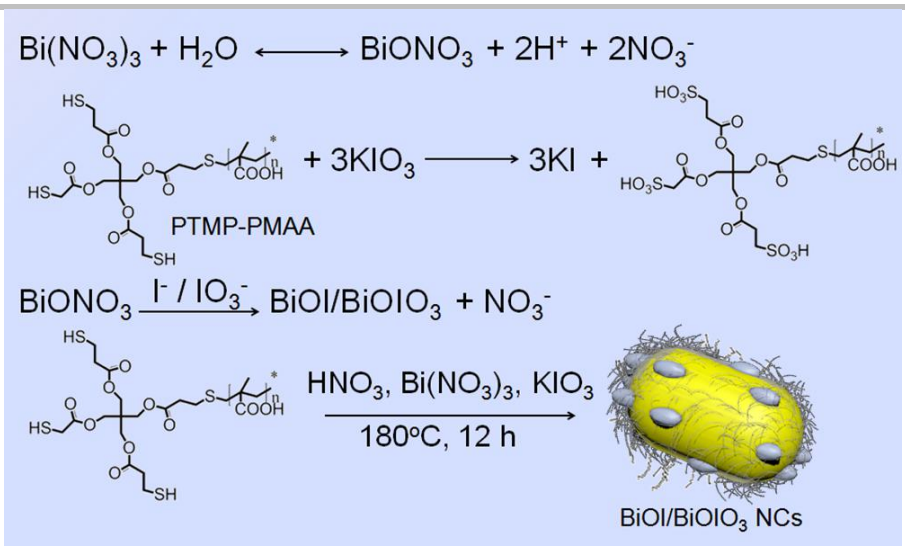

Fig. S3 Schematic illustration of synthetic process of BB NCs.

When bismuth nitrate pentahydrate was dispersed in the water, at the beginning, Bi^{3+} cations reacted with H_2O to form $Bi(OH)_2^+$, when the pH value of the precursor is suddenly decreased and then H^+ concentration increased, the reaction prefer to the left direction and finally decrease the amount of $Bi(OH)_2^+$ and $BiONO_3$,[4] which inhibits the growing of $BiONO_3$ into big size. The –SH of our used surfactant (PTMP-PMAA) can be reacted with KIO_3 and generate KI (Fig. S3).[5] $BiONO_3$ can be transformed to $BiOIO_3$ and BiOI by combined with IO_3^- and I^-, and the uniform $BiOI/BiOIO_3$ heterostructure nanocomposites (BB NCs) were prepared through this one step hydrothermal method.

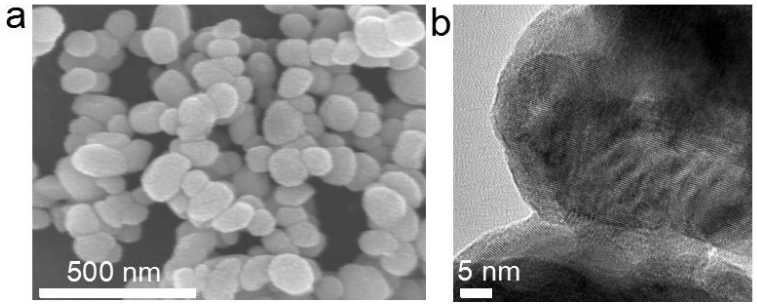

Fig. S4 (a) SEM image of BB NCs. (b) Enlarged TEM image of BB NCs.

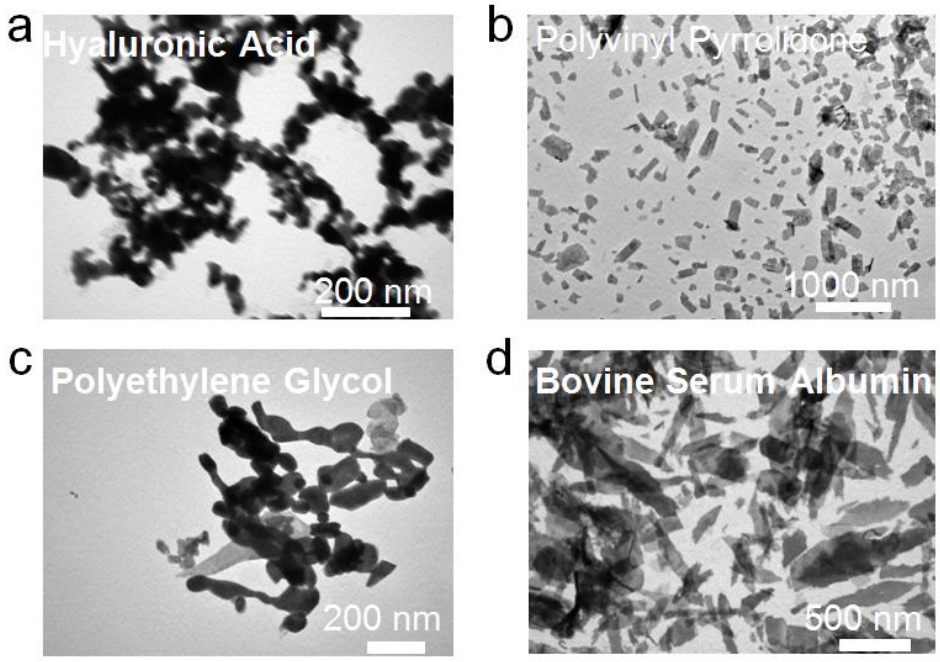

Fig. S5 TEM images of products prepared through the same procedures as BB NCs using different surfactants.

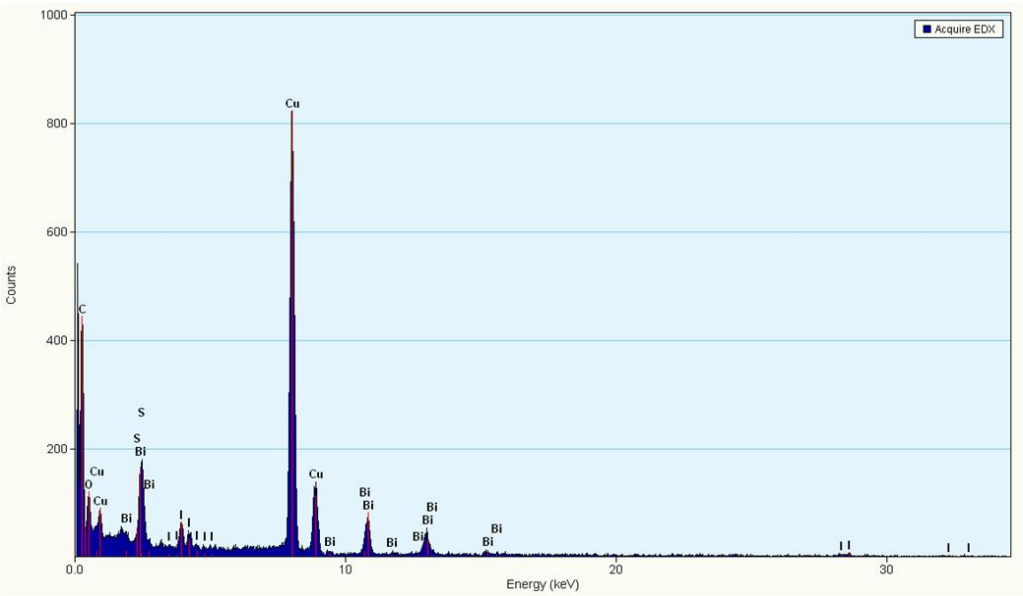

Fig. S6 EDS of BB NCs.

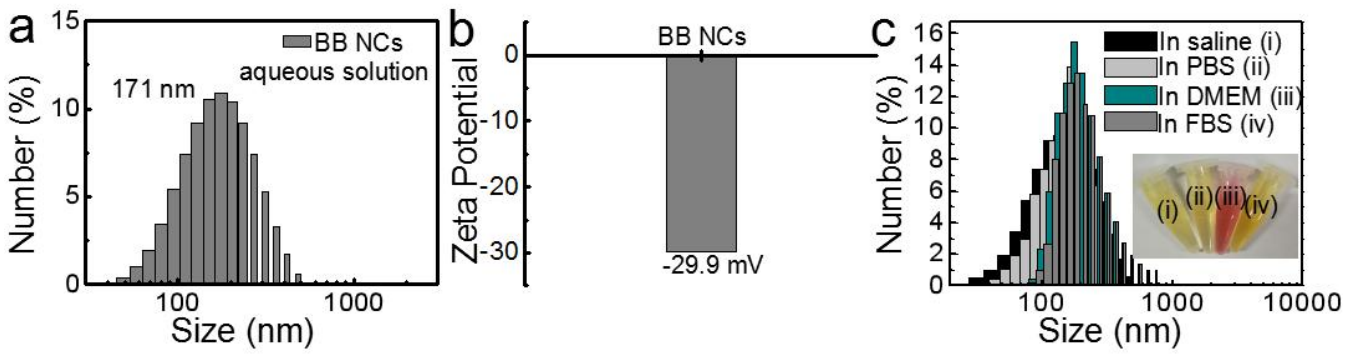

Fig. S7 Hydrodynamic size (a) and ξ-potential (b) of BB NCs aqueous solution. (c) Hydrodynamic size of BB NCs in saline, PBS, DMEM medium and 80% of FBS.

The as-prepared BB NCs disperse well in water, and the hydrodynamic size is about 171 nm (Fig. S7a) and ξ-potential of -29.9 mV (Fig. S7b). To further test the stability of the BB NCs in saline, PBS, DMEM medium and FBS, we dispersed BB NCs in saline, PBS, DMEM medium and 80% of FBS for 2 d. We measured their hydrodynamic size (Fig. S7c). The results are shown in Fig. S7c, BB NCs showed reasonable stability as the hydrodynamic size of BB NCs did not change apparently.

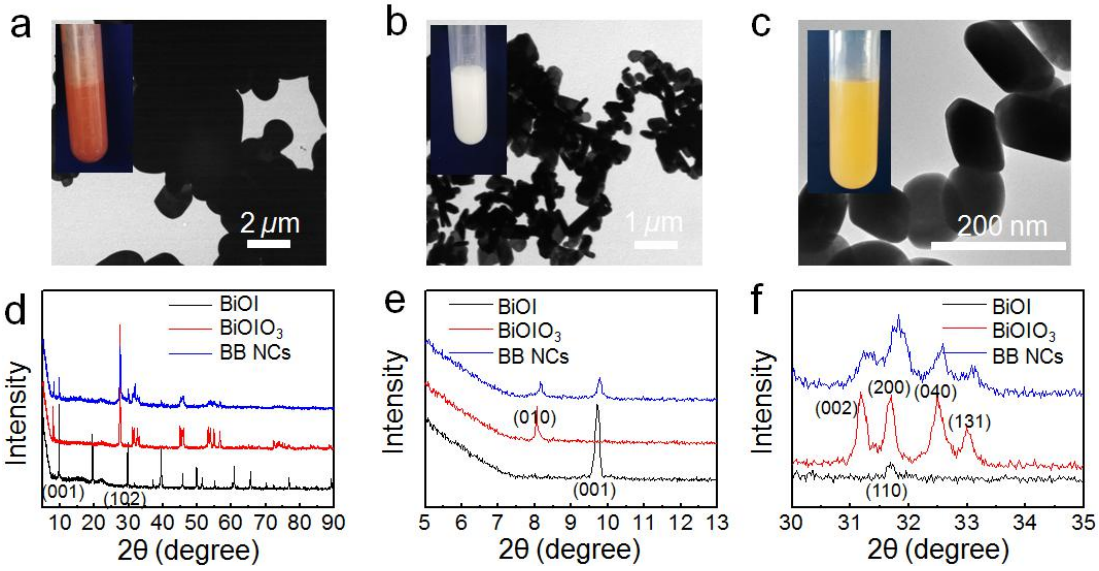

Fig. S8 TEM images and photos (insets) of BiOI (a), $BiOIO_3$ (b) and BB NCs (c). (d) XRD spectra of BiOI, $BiOIO_3$ and BB NCs. (e) Enlarged XRD spectra of BiOI, $BiOIO_3$ and BB NCs in the range of 5~13 degree. (f) Enlarged XRD spectra of BiOI, $BiOIO_3$ and BB NCs in the range of 30~35 degree.

To compare the structure of BB NCs to single $BiOIO_3$ and BiOI, we also prepared pure BiOI and $BiOIO_3$ which aqueous solution show brick red and white, respectively (Fig. S8a, b). From the XRD spectra (Fig. S8d-f) of our obtained BiOI (black line), $BiOIO_3$ (red line) and BB NCs (blue line), we can find that all of them have sharp diffraction peaks, indicating they were well crystallized. In addition, our obtained BiOI sample was in agreement with tetragonal phase of BiOI (JCPDS file 10-0445),[6] and the XRD peaks of our prepared $BiOIO_3$ was in good agreement with the orthorhombic $BiOIO_3$ (ICSD #

262019).[5] The XRD spectrum of BB NCs was also shown in Fig. S8d, both of the diffraction peaks of BiOI and $BiOIO_3$ can be observed. Most of the typical peaks of BB NCs are similar to those of $BiOIO_3$ except the appearance of the peaks at 9.658° and 29.645° belonging to (001) and (102) peaks of BiOI. Specifically, from the enlarged XRD spectra (Fig. S8e,f), the BB NCs have (010) peak compared with pure $BiOIO_3$, and the ratio of (040)/(002) is increased compared to that of pure $BiOIO_3$. Above XRD data suggests the coexistence of $BiOIO_3$ and BiOI.[6,7] According to the enlarged XRD spectra (Fig. S8e, S8f) ranging from 30-35 degree, the (010) and (040) peaks of BB NCs offset to a large angle to a certain extent compared to that of pure $BiOIO_3$, which comes from the absorption of BB NCs shifted towards the long wavelength.[7]

In addition, the HRTEM image (Fig. 1d) indicates that the lattice fringes with the interplanar space of 0.302 nm matching the spacing of the (102) crystal plane of BiOI, and 0.280 nm matching the spacing of the (110) crystal plane of BiOI, coupled with the XRD spectrum of BiOI (Fig. S8d-f), we can conclude that the main exposed facet of BiOI is {001} facet. The exposed {001} facets of BiOI can promote the photocatalytic activity, which comes from the effective separation of photogenerated e^-–h^+ on {001} facets.[7] Besides, the interplanar spacing of the clear lattice fringe of 0.287 nm is in accordance with the (002) crystal plane of $BiOIO_3$, combined with the XRD spectrum of $BiOIO_3$ (Fig. S8d), the dominantly exposing facet of $BiOIO_3$ may be {010} facet. From Fig. 1f, we can also conclude that the BiOI was formed on the surface of $BiOIO_3$, which suggests that the BiOI/$BiOIO_3$ heterostructures (BB NCs) were synthesized, the BiOI and $BiOIO_3$ layers contacted intimately. As it is reported that the {001} facet and {010} facet are the reactive crystal facets of BiOI and $BiOIO_3$, respectively,[6] the coupling of the two kinds of reactive crystal facets is beneficial to the separation and transfer of charge carriers.

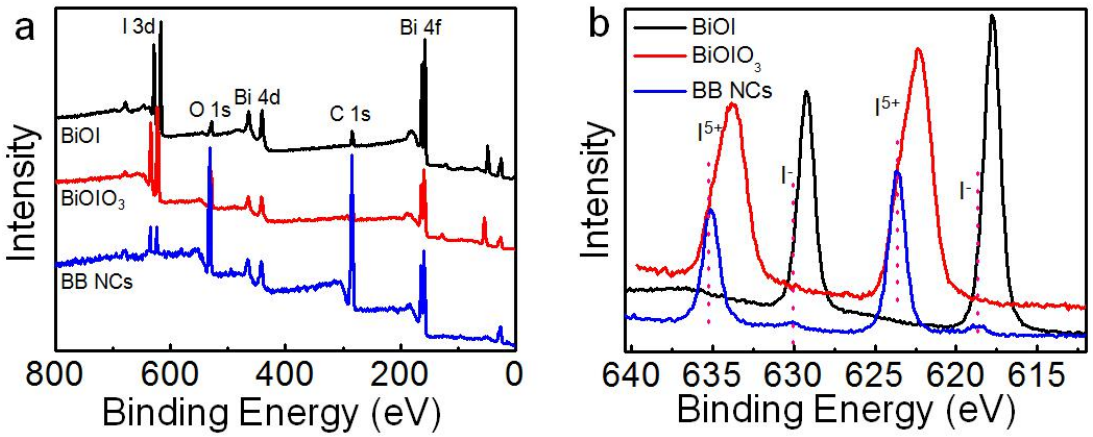

Fig. S9 XPS spectra of BiOI, $BiOIO_3$ and BB NCs.

The XPS spectra of $BiOIO_3$, BiOI and BB NCs were used to investigate the chemical compositions and surface states. The XPS survey spectra of $BiOIO_3$, BiOI and BB NCs indicate that the three samples contain Bi, O, I elements (Fig. S9). From Fig. S9a, two peaks around 164.1 and 158.74 eV are indexed to Bi $4f_{5/2}$ and Bi $4f_{7/2}$, indicating the presence of Bi^{3+} in $BiOIO_3$, BiOI and BB NCs.[7,8] And two peaks around 630.4 eV (I $3d_{3/2}$) and 618.9 eV (I $3d_{5/2}$) could be ascribed to the I^- in BiOI, two strong

peaks at 635.05 and 623.6 eV are the I $3d_{3/2}$ and I $3d_{5/2}$ states of I^{5+} in $BiOIO_3$ (Fig. S9a). From Fig. S9b, BB NCs show two sets of I_{3d} peaks, and the two strong peaks around 635.05 and 623.6 eV are the I $3d_{3/2}$ and I $3d_{5/2}$ states of I^{5+}, whereas the other two peaks at about 630.4 eV and 618.9 eV are the I $3d_{3/2}$ and I $3d_{5/2}$ states of I^-, and the I^{5+} and I^- ions were in $BiOIO_3$ and BiOI respectively, suggesting the coexistence of $BiOIO_3$ and BiOI in BB NCs.[5] Unlike simple mechanical mixing with no chemical bonding, compared with pure $BiOIO_3$ and BiOI, the binding energy of I in BB NCs shift towards high binding energy, suggested that the interaction between $BiOIO_3$ and BiOI at the composite interface did occur, and the XPS spectra can further illustrate the coexistence of $BiOIO_3$ and BiOI in BB NCs and the effective composites were formed between the two kinds of the materials.[7,9]

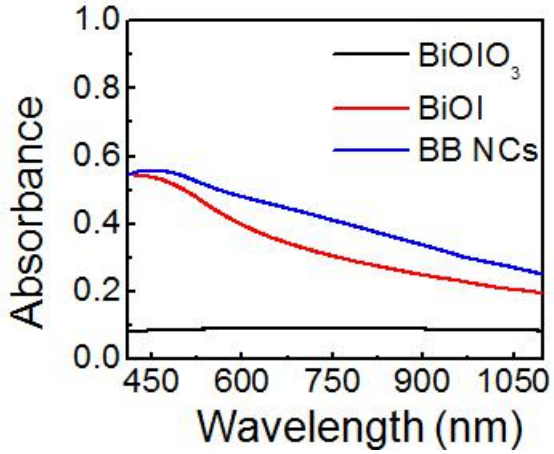

Fig. S10 UV-Vis absorbance of single $BiOIO_3$, BiOI and BB NCs.

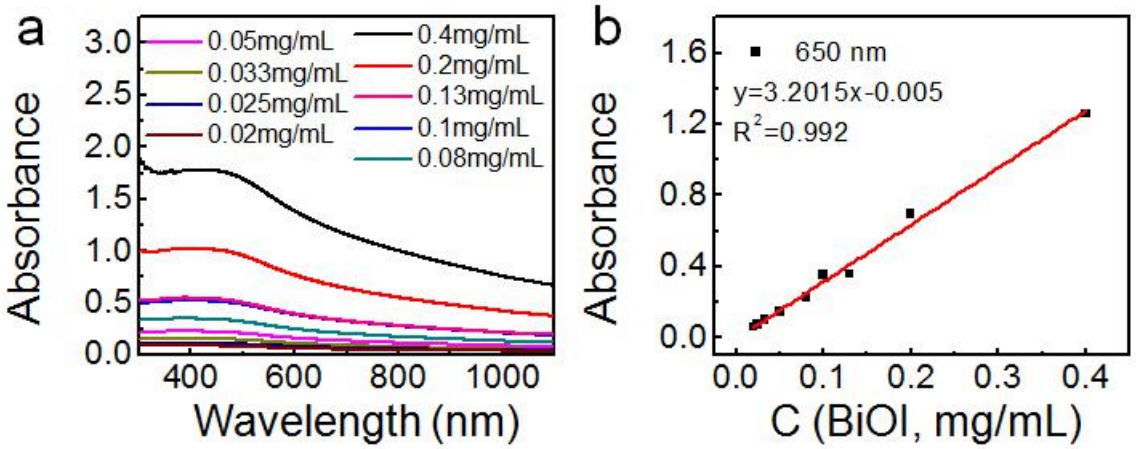

Fig. S11 (a) UV-Vis absorbance of single BiOI with different concentrations (BiOI was dispersed in 10 mL of deionized (D.I.) water and disrupted by ultrasonic disruption system (300 W) for 15 min). (b) Standard curve of BiOI.

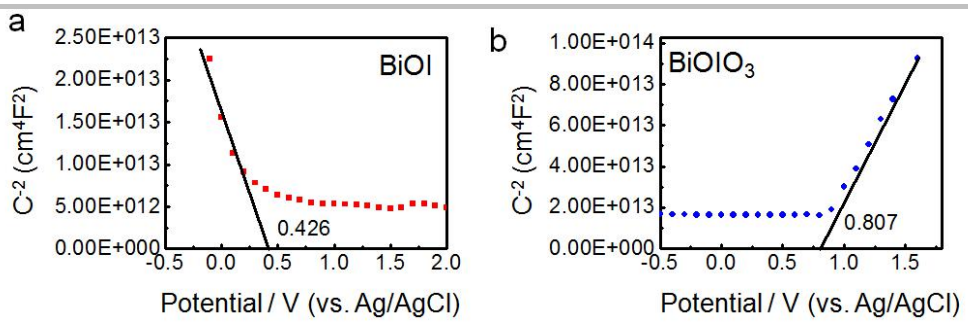

Fig. S12 Mott-Schottky plots of BiOI (a) and $BiOIO_3$ (b) performed in 1 mol L^{-1} Na_2SO_4 with frequency of 3000 Hz.

The optical properties have been confirmed by UV–vis diffuse reflectance spectroscopy (Fig. 2a). For a semiconductor, the band gap energy is described by the following equation: $\alpha h\upsilon = A(h\upsilon - Eg)^n$, where α, Eg, υ, and h represent absorbance, band gap, photon frequency, and Planck's constant.[6] According to Fig. 2b, the band gap energies of $BiOIO_3$ and BiOI are 3.05 eV and 1.70 eV respectively. And BB NCs can be stimulated by 650 nm whose light energy (2.006 eV) is higher than the band gap of BB NCs (1.76 eV). Whatsmore, it is reported that the valence band-edge potential of a semiconductor can be calculated by the empirical equation: $E_{VB} = X - E^e + 0.5E_g$,[5] X is the electronegativity of the semiconductor atoms, E_e is the energy of free electrons on the hydrogen scale (~4.5 eV), and E_g is the band gap energy of semiconductor. The CB bottom E_{CB} can be determined by $E_{CB} = E_{VB} - Eg$. The X value of $BiOIO_3$ is about 7.04 eV, so the E_{VB} is calculated to be 4.07 eV, and E_{CB} is calculated to be 1.02 eV. For BiOI, the X value is 5.99 eV, the E_{VB} is calculated to be 2.34 eV, and E_{CB} is calculated to be 0.64 eV. And the schematic band diagram of BiOI and $BiOIO_3$ was shown in Fig. 2c.[9]

M-S method can be employed to determine the semiconductor types of $BiOIO_3$ and BiOI as well as their flat band potential (E_{fb}). The slope of linear C^{-2} vs potential curves is positive for n-type semiconductor and negative for p-type semiconductor. As shown in Fig. S12a, b, the slope of linear C^{-2}-potential curves of BiOI and $BiOIO_3$ is separately positive and negative, demonstrating that $BiOIO_3$ and BiOI are n-type semiconductor and p-type semiconductor, respectively. Therefore, BiOI and $BiOIO_3$ could form a p-n heterojunction. By extrapolation to $C^{-2} = 0$, the flat potentials of BiOI and $BiOIO_3$ are separately determined to be 0.426 and 0.807 V (*vs* Ag/AgCl, namely, 0.633 V and 1.014 V *vs* NHE). The CB bottom E_{CB} can be determined by $E_{VB} = E_{CB} + Eg$. The E_{VB} of BiOI and $BiOIO_3$ are 2.333 eV and 4.064 eV (*vs* NHE)), respectively.

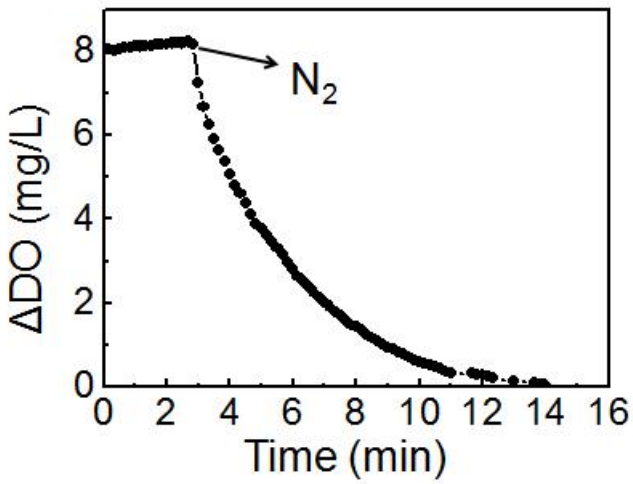

Fig. S13 Variation of the dissolved oxygen after the administration of N_2.

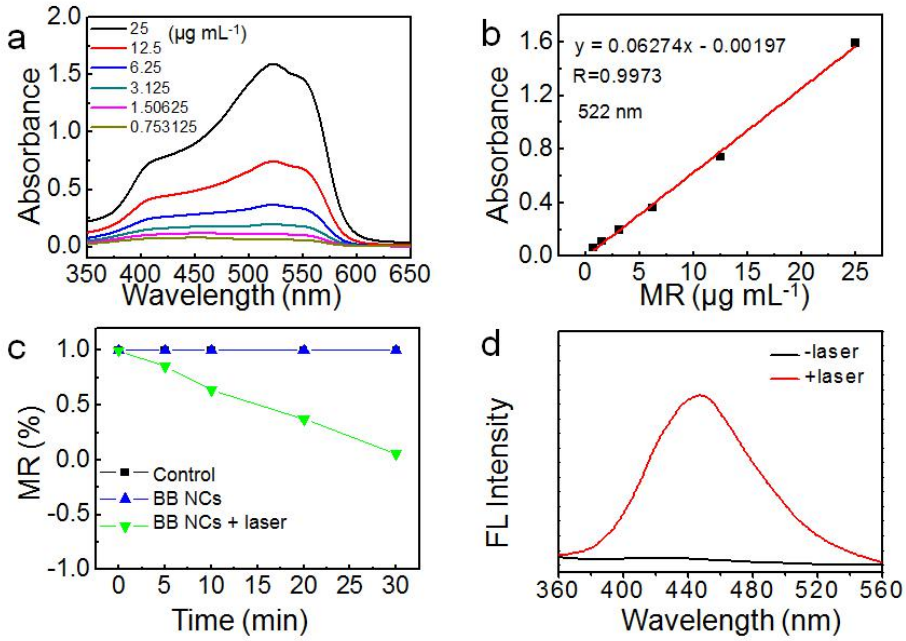

Fig. S14 (a) The UV-Vis spectra of MR with different concentrations. (b) Standard curve of MR. (c) Photodegration of MR under irradiation of 650 nm (0.5 W cm^{-2}) with BB NCs (80 μg mL^{-1}). (d) The FL spectra of TA after the irradiation of 650 nm (0.5 W cm^{-2}) with BB NCs (80 μg mL^{-1}).

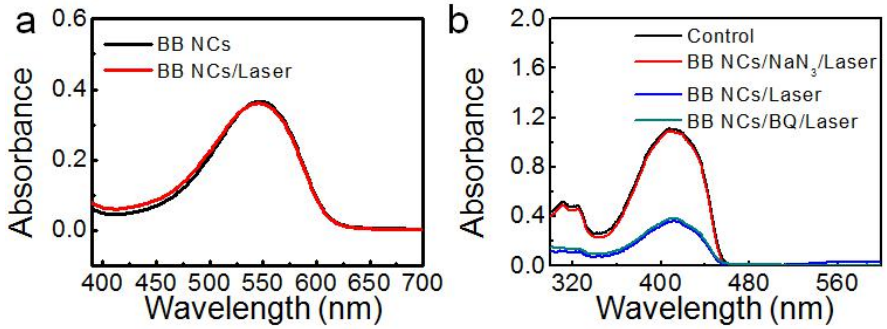

Fig. S15 (a) Detection of $\bullet O_2^-$. (b) Consumption of DPBF in different treatments.

From Fig. S15a, we used "inhibition and produce superoxide anion assay kit" to detect $\bullet O_2^-$, no significant change was discovered. It demonstrates that our prepared BB NCs can't generate $\bullet O_2^-$, which is in accordance with the schematic band diagram theory (Fig. 2c, E_{CB} is higher than the E_0 of O_2 /$\bullet O_2^-$ (-0.05 eV)). To further demonstrate that BB NCs can generate $^1O_2$ and the BB NCs can't generate $\bullet O_2^-$, we used DPBF (a chemical trapping probe whose absorption at 410 nm would be decreased upon its irreversible reaction with $^1O_2$ and $\bullet O_2^-$) to detect $^1O_2$ or $\bullet O_2^-$. Obviously, we found that the absorption of DPBF was significantly decayed in BB NCs solution under the irradiation of 650 nm laser (Fig. S1b), suggesting that BB NCs can generate $^1O_2$ or $\bullet O_2^-$. While we used the NaN_3 to scavenge the $^1O_2$, the absorbance of DPBF was not decayed, and while we used BQ to scavenge the $\bullet O_2^-$, the ratio of decayed DPBF was not changed compared to the BB NCs/Laser group, suggesting that can generate $^1O_2$ and the BB NCs can't generate $\bullet O_2^-$.

Table 1. Comparison of the X-ray attenuation coefficient of present work.

Z number	Element	Nanomaterials	X-ray attenuation coefficient	Ref
42	Mo	$MoSe_2$ hetero-dimensional hybrid (HDH)	45.69 HU L g^{-1}	R10
42	Mo	Hollow MoS_x	17.94 HU L g^{-1}	R11
53	I	Iohexol	51.81 HU L g^{-1}	R12
53	I	Iopromide	16.4 HU L g^{-1}	R13
55, 74	Cs, W	Cs_xWO_3 NR@PEM	68.48 HU L g^{-1}	R12
70	Yb	GdOF:Ln@SiO_2	123.58 HU L g^{-1}	R14
73	Ta	polymer-coated TaOx NPs	6.0 HU mM^{-1}	R15
74	W	WS_2:Gd^{3+} PEG	25.9 HU L g^{-1}	R16
74	W	WS_2 quantum dots	37.73 HU L g^{-1}	R17
74	W	Rb_xWO_3 Nanorods	38.66 HU L g^{-1}	R18
75	Re	rhenium trioxide nanocu bes	10.82 HU mM^{-1}	R19
77	Ir	IrO_2	11.51 HU mM^{-1}	R20
79	Au	Au@MSNs-ICG NPs	38.00 HU L g^{-1}	R21
79, 78	Au, Pt	Au@Pt Nanodendrites	28.6 HU L g^{-1}	R22

83	Bi	PVP-coated Bi_2S_3	9.3 HU mM^{-1}	R23
83	Bi	BB NCs	41.39 HU L g^{-1}	This work

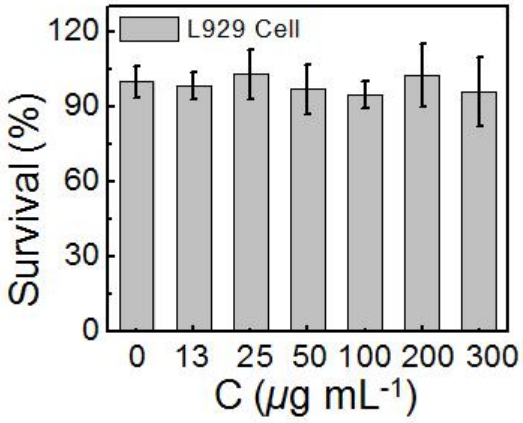

Fig. S16 Survival rate of L929 cells after incubated with BB NCs with different concentrations for 24 h under normoxia condition.

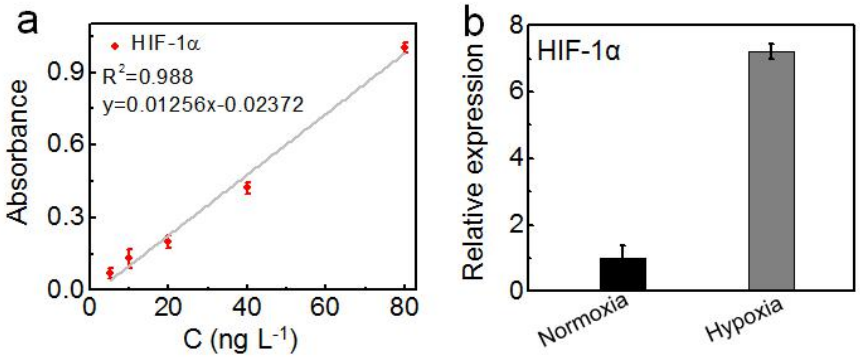

Fig. S17 (a) Standard curve of HIF-1α. (b) Variation of the HIF-1α after HeLa cells incubated at hypoxia condition (2% O_2) and normoxia condition (21% O_2).

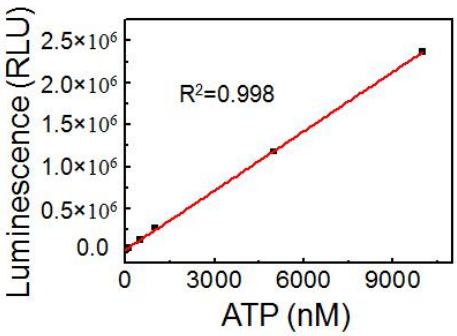

Fig. S18 Standard curve of ATP.

Table 2. The dose of present type I PDT photocatalytic nanomaterials used at in vivo tumor model.

Type of PDT	Nanomaterials	Laser	Dose	Dose ($mg\ kg^{-1}$)	Ref
I	BiOI@Bi_2S_3@BSA	X-ray	20 µL, 2 mg mL^{-1}	1.6	R24
	CeIII-doped $LiYF_4$@SiO_2@ZnO structure	X-ray	100 µL, 1 mg mL^{-1}	4	R25
	Hollow cerium oxide upconversion nanoparticles	980 nm (Not Given), 20 min	200 µL, 0.1 mg mL^{-1}	0.8	R26
	TiO_2@$Y_2Ti_2O_7$@ YOF:Yb,Tm	980 nm (0.72 W cm^{-2}), 10 min	100 µL, 1 mg mL^{-1}	4	R27
	Fe@γ-Fe_2O_3@H-TiO_2 Nanocomposites	808 nm (2 W cm^{-2}), 5 min	100 µL, 2 mg mL^{-1}	8	R28
	(UCNPs)@TiO_2@MnO_2 core/shell/sheet nanocomposites	980 nm (2 W cm^{-2}), 10 min	200 µL, 1 mg mL^{-1}	8	R29
	bismuth ferrite nanoparticles	880 nm (2 W cm^{-2}), 10 min	100 µL, 3 mg mL^{-1}	12	R30
	(G-TiO_{2-x}-TPP)	980 nm (0.72 W cm^{-2}), 5 min	Not Given	8	R31
	(UCNPs)-platinum(IV) (Pt(IV))-$ZnFe_2O_4$	980 nm (0.5 W cm^{-2}), 15 min	100 µL, 4 mg mL^{-1}	16	R32
II	$Cu_2(OH)PO_4$@PAA QDs	1064 nm (2 W cm^{-2}), 10 min	100 µL, 1 mg mL^{-1}	4	R33
	metal–organic frameworks and	980 nm (1.2 W cm^{-2}), 5 min	Not Given	59	R34

	lanthanide-doped upconversion nanoparticles				
	PEGylated $W_{18}O_{49}$ Nanowires	880 nm (0.2 W cm^{-2}), 10 min	Not Given	15	R35
	Tellurium Nanodots	785 nm (1.5 W cm^{-2}), 5 min	Not Given	50 μmol kg^{-1}	R36
	BSA-IrO_2 nanoparticles	808 nm (1 W cm^{-2}), 10 min	200 μL, 1.5 mmol L^{-1}	12 μmol kg^{-1}	R20
	copper ferrite nanospheres	650 nm (0.469 W cm^{-2}), 10 min	300 μL, 0.2 mg mL^{-1}	2.4	R37
I	BB NCs	650 nm (0.5 W cm^{-2}), 15 min	200 μL, 0.08 mg mL^{-1}	0.64	This work

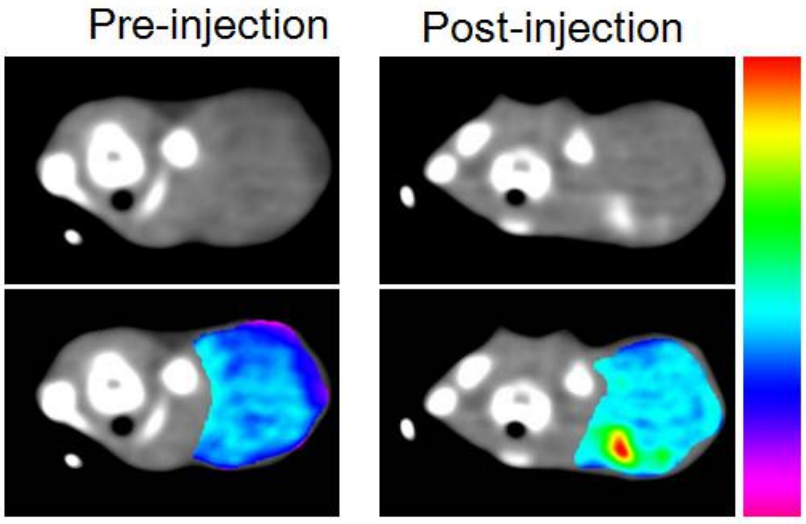

Fig. S19 2D CT images of tumor-bearing mice before and after injection of BB NCs.

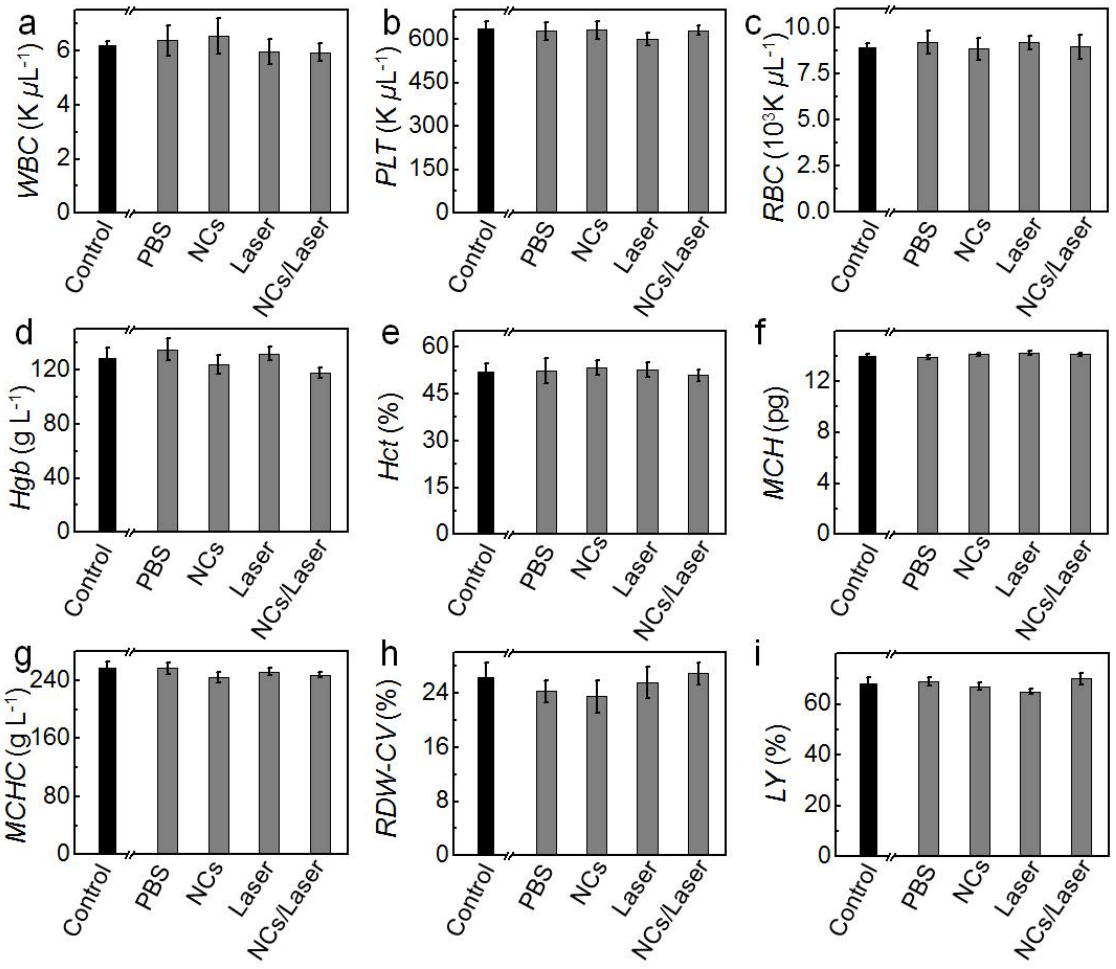

Fig. S20 Hematology analysis of mice with different treatments.

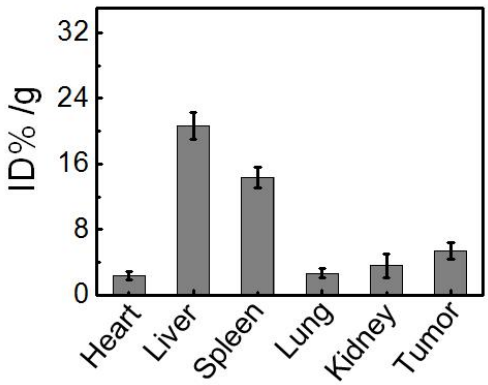

Fig. S21 Tissue distribution of BB NCs.

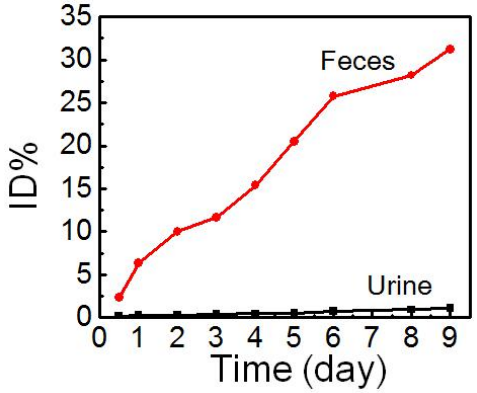

Fig. S22 Total content of BB NCs in urine and feces collected at various time points after intravenous injection.

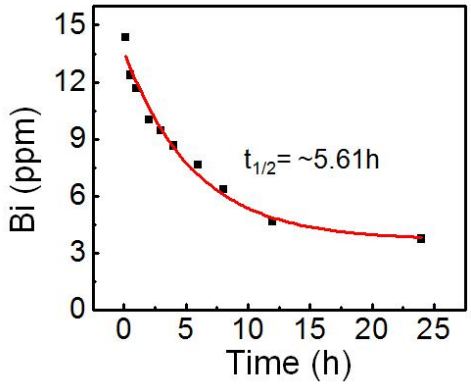

Fig. S23 Concentration of Bi element in blood after intravenous injection at different time points.

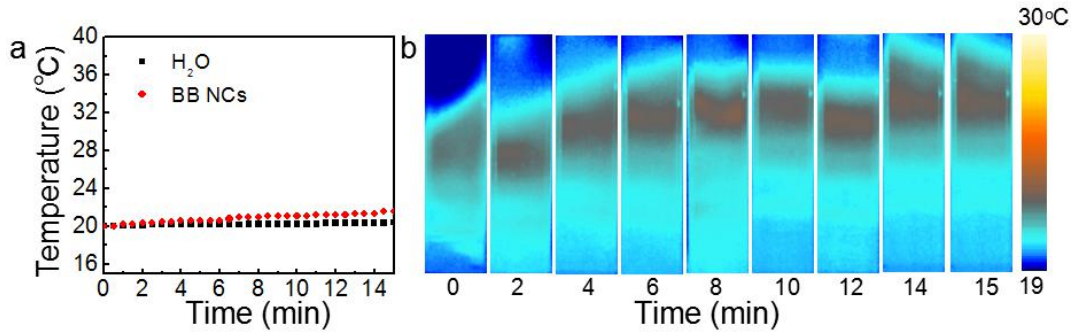

Fig. S24 (a) Temperature variation of H_2O and BB NCs aqueous solution (80 μg mL^{-1}) upon the irradiation of laser (650 nm, 0.5 W cm^{-2}) for 15 min. (b) Thermal imaging of BB NCs aqueous solution (80 μg mL^{-1}) under the illumination of laser at different time points.

To guarantee light power density we used will not produce the photothermal response and complicate the phototherapeutic outcome, the variation of temperature of BB NCs under the illumination of 650 nm laser at 0.5 Wcm^{-2} was evaluated. As shown in Fig. S24, compared to the H_2O group, the BB NCs aqueous solution don't have significant increasement of temperature.

References

[1] H. O. Ha, D. S. Kim, J. *Appl. Polym. Sci.* **2016**, *133*, 1-7.

[2] S. A. Jabin, *J. Bangladesh, Sci. Ind. Res.* **2009**, *44*, 225-228.

[3] F. J. R. Hird, J. R. Yates, *Biochem. J.* **1961**, *80*, 612-616.

[4] X. M. Qi, M. L. Gu, X. Y. Zhu, J. Wu, H. M. Long, K. He, Q. Wu, *Chem. Eng. J.* **2016**, *285*, 11-19.

[5] F. Dong, T. Xiong, Y. Sun, Y. Zhang, Y. Zhou, *Chem. Commun.* **2015**, *51*, 8249-8252.

[6] H. Huang, K. Xiao, K. Liu, S. Yu, Y. Zhang, *Cryst. Growth Des.* **2016**, *16*, 221-228.

[7] R. Zhou, J. Wu, J. Zhang, H. Tian, P. Liang, T. Zeng, P. Lu, J. Ren, T. Huang, X. Zhou, P. Sheng, *Appl. Catal. B-Environ.* **2017**, *204*, 465-474.

[8] (a) K. H. Reddy, S. Martha, K. M. Parida, *Inorg. Chem*. **2013**, *52*, 6390-6401; (b) W. He, H. Jia, W. G. Wamer, Z. Zheng, P. Li, J. H. Callahan, J. Yin, *J. Catal.* **2014**, *320*, 97-105; (c) H. He, S. P. Berglund, P. Xiao, W. D. Chemelewski, Y. Zhang, C. B. Mullins, *J. Mater. Chem. A*, **2013**, *1*, 12826-12834; (d) S. Zhang, J. Li, X. Wang, Y. Huang, M. Zeng, J. Xu, *J. Mater. Chem. A*, **2015**, *3*, 10119-10126; d) X. Yu, S. Wang, X. Zhang, A. Qi, X. Qiao, Z. Liu, M. Wu, L. Li, Z. Wang, *Nano Energy* **2018**, *46*, 29-38.

[9] X. Sun, J. Wu, Q. Li, Q. Liu, Y. Qi, L. You, Z. Ji, P. He, P. Sheng, J. Ren, W. Zhang, J. Lu, J. Zhang, *Appl. Cat. B-Environ.* **2017**, *218*, 80-90.

[10] B. Mao, T. Bao, J. Yu, L. Zheng, J. Qin, W. Yin, M. Cao, *Nano Res.* **2017**, *10*, 2667-2682.

[11] J. Wang, L. Liu, Q. You, Y. Song, Q. Sun, Y. Wang, Y. Cheng, F. Tan, N. Li, *Theranostics* **2018**, *8*, 955-971.

[12] W. Guo, C. Guo, N. Zheng, T. Sun, S. Liu, *Adv. Mater.* **2017**, *29*, 1604157.

[13] Z. Li, J. Liu, Y. Hu, K. A. Howard, Z. Li, X. Fan, M. Chang, Y. Sun, F. Besenbacher, C. Chen, M. Yu, *ACS Nano* **2016**, *10*, 9646-9658.

[14] R. Lv, P. Yang, F. He, S. Gai, C. Li, Y. Dai, G. Yang, J. Lin, *ACS Nano*, **2015**, *9*, 1630-1647.

[15] M. H. Oh, N. Lee, H. Kim, S. P. Park, Y. Piao, J. Lee, S. W. Jun, W. K. Moon, S. H. Choi, T. Hyeon, *J. Am. Chem. Soc.* **2011**, *133*, 5508-5515.

[16] L. Cheng, C. Yuan, S. Shen, X. Yi, H. Gong, K. Yang, Z. Liu, *ACS Nano*, **2015**, *9*, 11090-11101.

[17] Y. Yong, X. Cheng, T. Bao, M. Zu, L. Yan, W. Yin, C. Ge, D. Wang, Z. Gu, Y. Zhao, *ACS Nano*, **2015**, *9*, 12451-12463.

[18] G. Tian, X. Zhang, X. Zheng, W. Yin, L. Ruan, X. Liu, L. Zhou, L. Yan, S. Li, Z. Gu, Y. Zhao, *Small* **2014**, *10*, 4160-4170.

[19] W. Zhang, G. Deng, B. Li, X. Zhao, T. Ji, G. Song, Z. Xiao, Q. Cao, J. Xiao, X. Huang, G. Guan, R. Zou, X. Lu, J. Hu, *Biomaterials* **2018**, *159*, 68-81.

[20] W. Zhen, Y. Liu, L. Lin, J. Bai, X. Jia, H. Tian, X. Jiang, *Angew. Chem. Int. Ed.* **2018**, *57*, 10309-10313.

[21] C. Zeng, W. Shang, X. Liang, X. Liang, Q. Chen, C. Chi, Y. Du, C. Fang, J. Tian, *ACS Appl. Mater. Inter.* **2016**, *8*, 29232-29241.

[22] X. Liu, X. Zhang, M. Zhu, G. Lin, J. Liu, Z. Zhou, X. Tian, Y. Pan, *ACS Appl. Mater. Inter.* **2017**, *9*, 279-285.

[23] O. Rabin, J. M. Perez, J. Grimm, G. Wojtkiewicz, R. Weissleder, *Nat. Mater.* **2006**, *5*, 118-122.

[24] Z. Guo, S. Zhu, Y. Yong, X. Zhang, X. Dong, J. Du, J. Xie, Q. Wang, Z. Gu, Y. Zhao, *Adv. Mater.* **2017**, *29*, 1704136.

[25] C. Zhang, K. Zhao, W. Bu, D. Ni, Y. Liu, J. Feng, J. Shi, *Angew. Chem. Int. Ed.* **2015**, *54*, 1770-1774.

[26] C. Yao, W. Wang, P. Wang, M. Zhao, X. Li, F. Zhang, *Adv. Mater.* **2018**, *30*, 1704833.

[27] R. Lv, C. Zhong, R. Li, P. Yang, F. He, S. Gai, Z. Hou, G. Yang, J. Lin, *Chem. Mater.* 2015, 27, 1751-1763.

[28] M. Wang, K. Deng, W. Lü, X. Deng, K. Li, Y. Shi, B. Ding, Z. Cheng, B. Xing, G. Han, Z. Hou, J. Lin, *Adv. Mater.* **2018**, *30*, 1706747.

[29] C. Zhang, W. Chen, L. Liu, W. Qiu, W. Yu, X. Zhang, *Adv. Funct. Mater.* **2017**, *27*, 1700626.

[30] C. Yang, Y. Chen, W. Guo, Y. Gao, C. Song, Q. Zhang, N. Zheng, X. Han, C. Guo, *Adv. Funct. Mater.* **2018**, *28*, 1706827.

[31] J. Mou, T. Lin, F. Huang, J. Shi, H. Chen, *Theranostics* **2017**, *7*, 1531-1542.

[32] H. Bi, Y. Dai, P. Yang, J. Xu, D. Yang, S. Gai, F. He, B. Liu, C. Zhong, G. An, J. Lin, *Small* **2018**, *14*, 1703809.

[33] W. Guo, Z. Qiu, C. Guo, D. Ding, T. Li, F. Wang, J. Sun, N. Zheng, S. Liu, *ACS Appl. Mater. Inter.* **2017**, *9*, 9348-9358.

[34] Y. Li, Z. Di, J. Gao, P. Cheng, C. Di, G. Zhang, B. Liu, X. Shi, Li. Sun, L. Li, C. Yan, *J. Am. Chem. Soc*. **2017**, *139*, 13804-13810.

[35] P. Kalluru, R. Vankayala, C. Chiang, K. C. Hwang, *Angew. Chem. Int. Ed.* **2013**, *52*, 12332-12336.

[36] T. Yang, H. Ke, Q. Wang, Y. Tang, Y. Deng, H. Yang, X. Yang, P. Yang, D. Ling, C. Chen, Y. Zhao, H. Wu, H. Chen, *ACS Nano* **2017**, *11*, 10012-10024.

[37] Y. Liu, W. Zhen, L. Jin, S. Zhang, G. Sun, T. Zhang, X. Xu, S. Song, Y. Wang, J. Liu, H. Zhang, *ACS Nano* **2018**, *12*, 4886-4893.